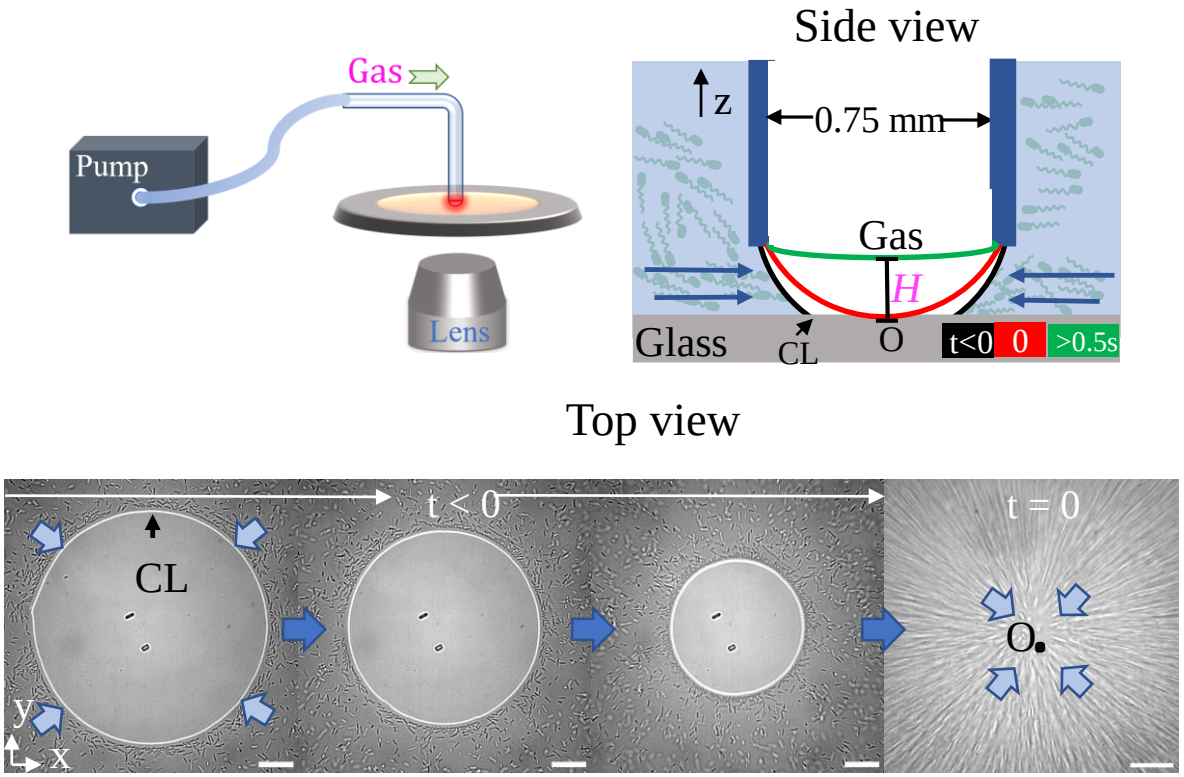

Fig. S1: A converging water-air-solid contact line (CL) aligns swimming bacteria. $t = 0$ marks the moment when the CL coalesces at the center O. H denotes the final height of the water-air interface above the substrate. Snapshots of experiment at different times show the CL moving toward the center in a dilute suspension of bacteria ($\rho = 2 \times 10^{10}\ /mL$). Scale bars, 20 μm.

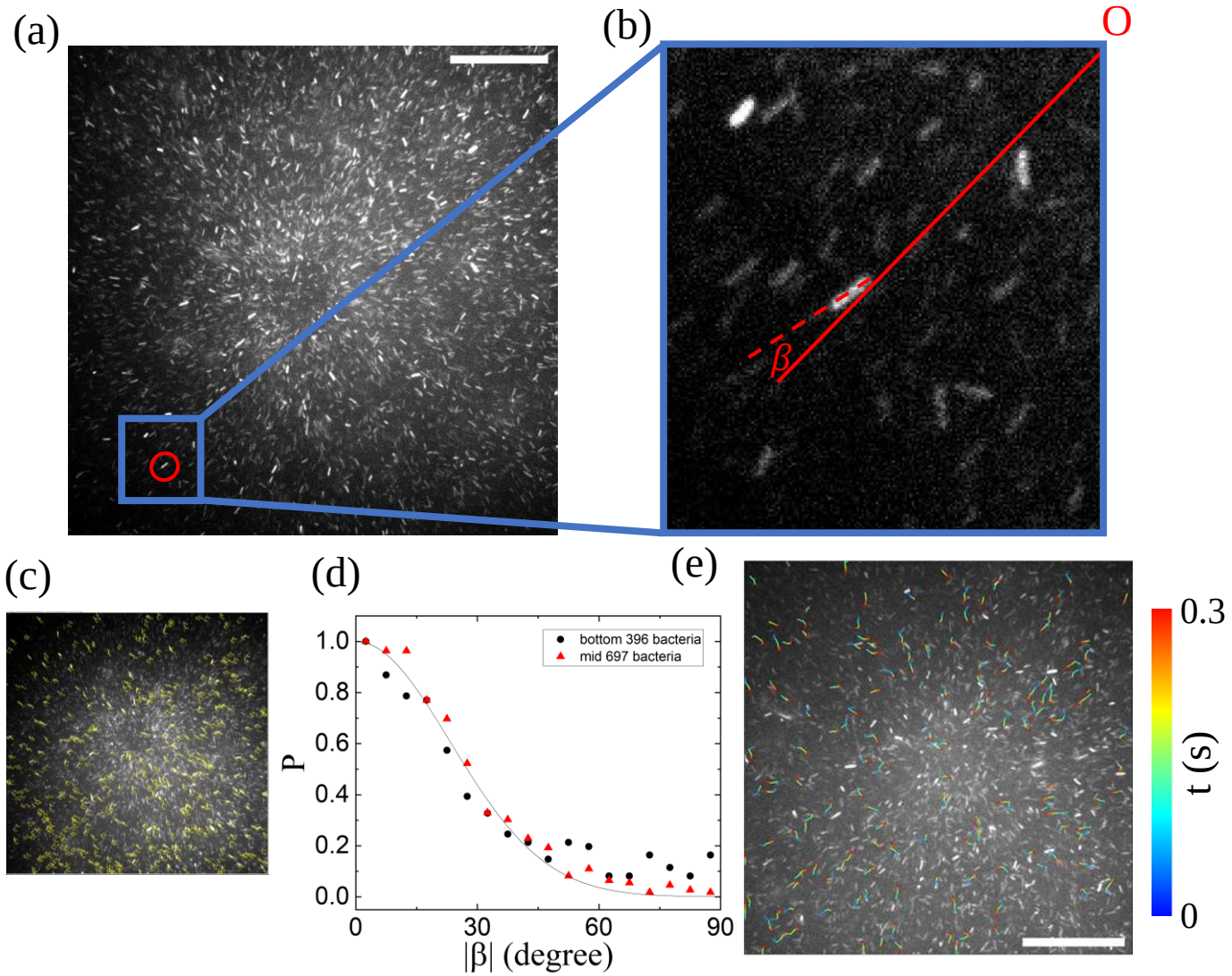

Fig. S2: Bacterial orientations in Phase I. (a) Snapshot at *t=0.1 s*, using fluorescently labeled bacteria mixed with wild-type bacteria. The bacterial fluid thickness is $H \approx 70\ \mu m$, captured above the bottom plate. Total bacterial concentration is $\rho \sim 2 \times 10^{11}/mL$. (b) Definition of the orientation angle β. The red dashed line marks the bacterial body axis and the red solid line connects the bacterium to the center O. (c) Example of bacteria sampled for analysis. (d) Probability distribution of $|\beta|$, measured at two different focal heights in two independent experiments, both with $H \approx 70\ \mu m$. The number of analyzed bacteria is indicated. The black solid line shows a Gaussian fit with a standard deviation of 33°. (e) Bacterial trajectories. Scale bars: 30 μm.

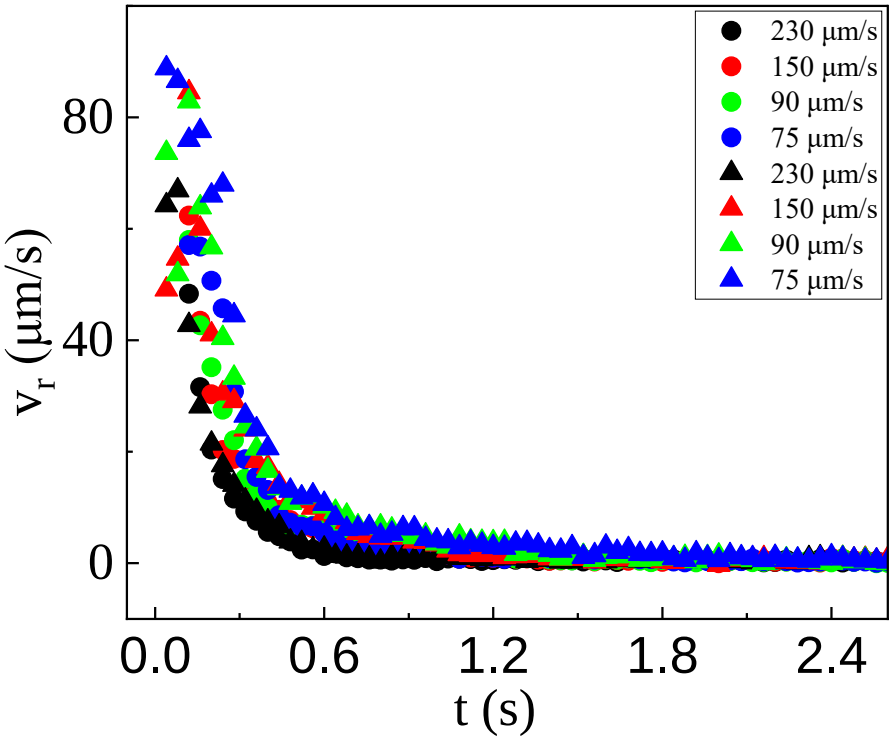

Fig. S3: Inward radial speed in suspensions of immobile bacteria after CL coalesces at *t=0*. Circles and triangles represent measurements at radial distances of r=14 and 31.5 μm from the center O, respectively. Colors indicate CL speed prior to *t=0*. All data were acquired 7 μm above the substrate. The shear rate is estimated as $\dot{\gamma} = (80\ \mu m/s)/7\mu m > 10\ s^{-1}$, with the shear gradient along the vertical direction.

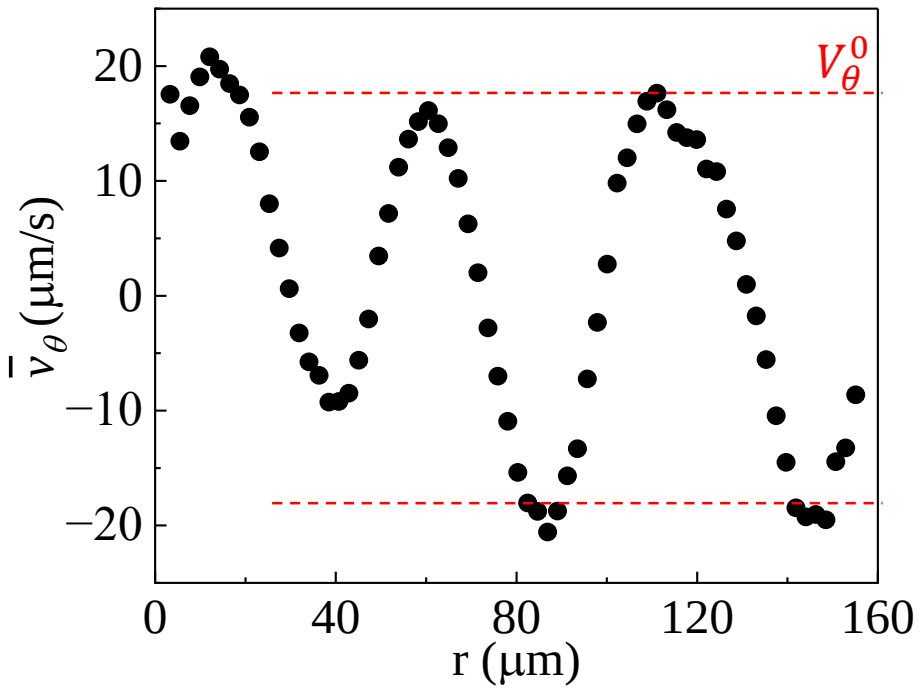

Fig. S4: Azimuthal average of the tangential velocity of bacterial flow at different radial positions. The red dashed lines indicate the amplitude V_θ^0. Same experiment in Fig. 1(c).

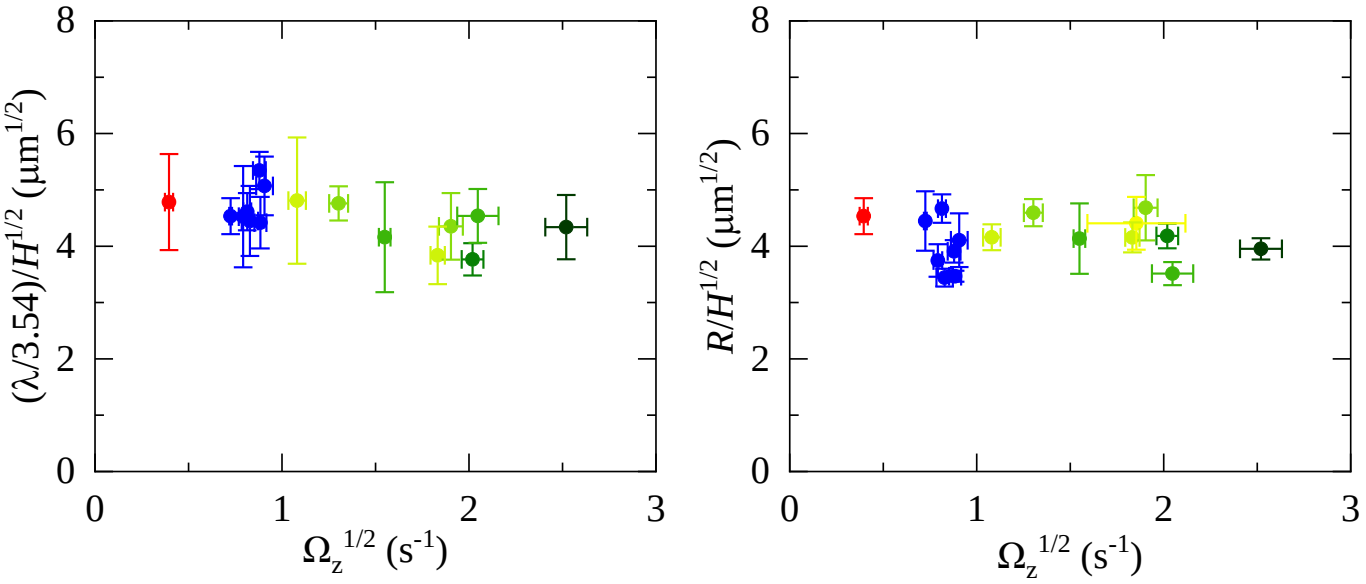

Fig. S5: Characteristic length scales, normalized by $H^{1/2}$, as functions of activity. The mean values for the three activity groups are shown in Fig.3(d).

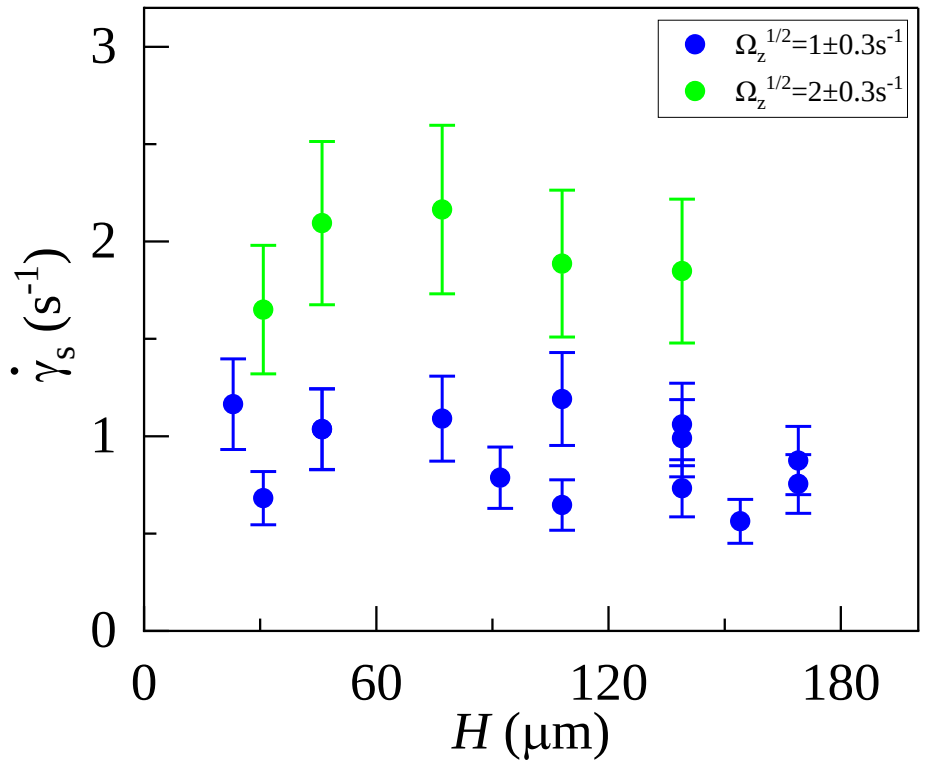

Fig. S6: Self-shear rate as a function of fluid thickness H at two activity levels. Same data as in Fig. 4(f).

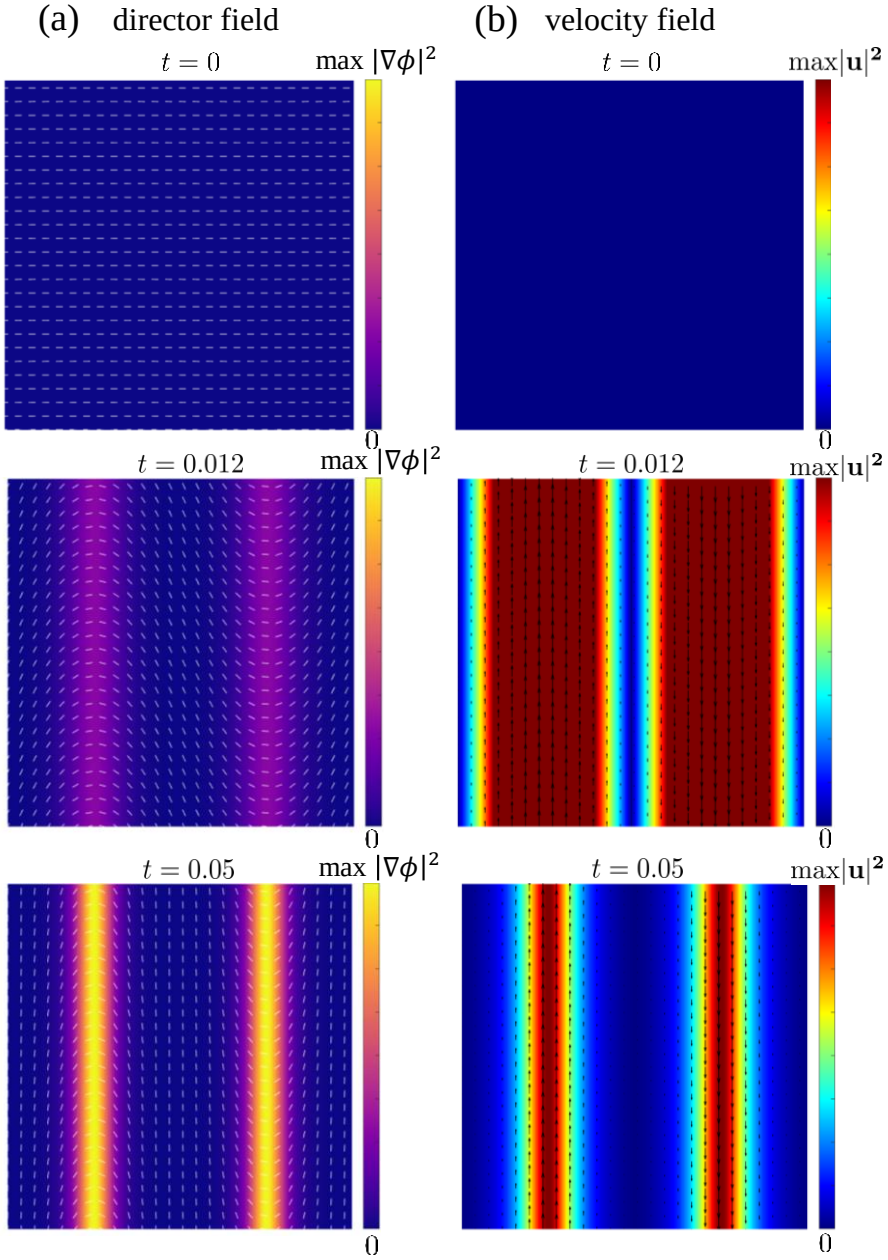

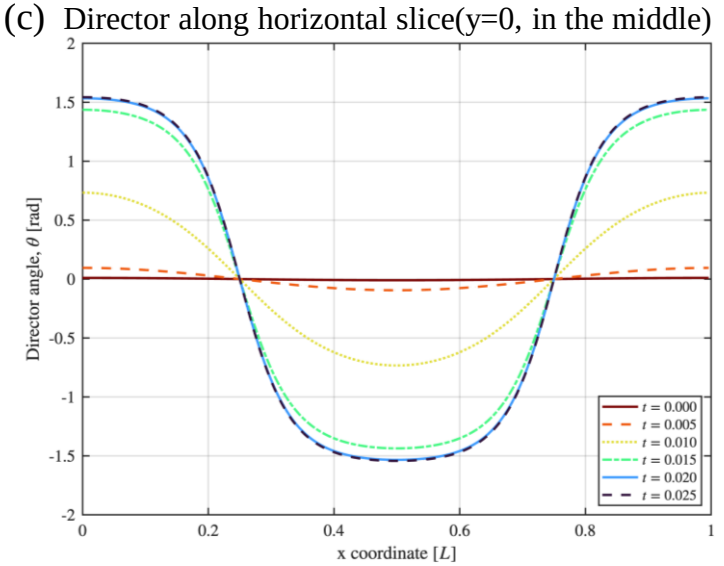

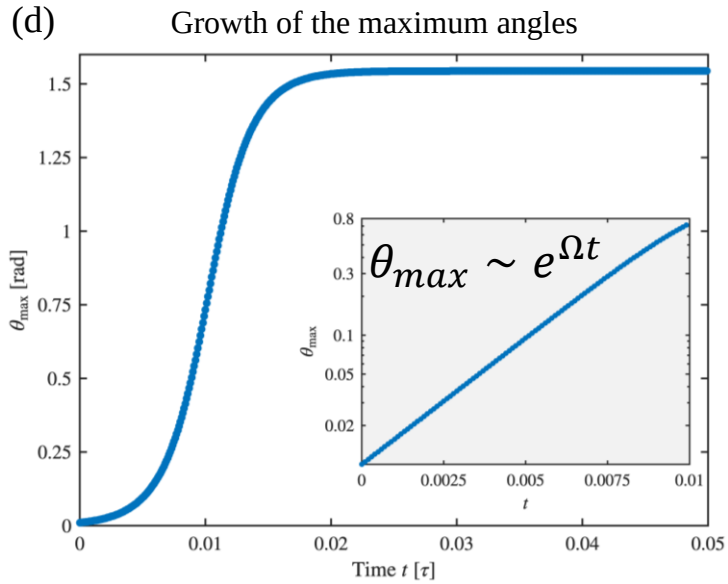

Fig.S7: Numerical verification. (a) Director field $\mathbf{n} = (\cos\phi, \sin\phi)$ at three representative times. Color bar shows the Frank energy density, $|\nabla\phi|^2$. A=1000. (b) Velocity field $\mathbf{u} = (u, v)$ at the same times. Color bar indicates the velocity magnitude. (c) Director vector along the horizontal slice at $y = 0$ at different times. (d) Temporal evolution of the maximum director angle. Inset: exponential growth at early times.

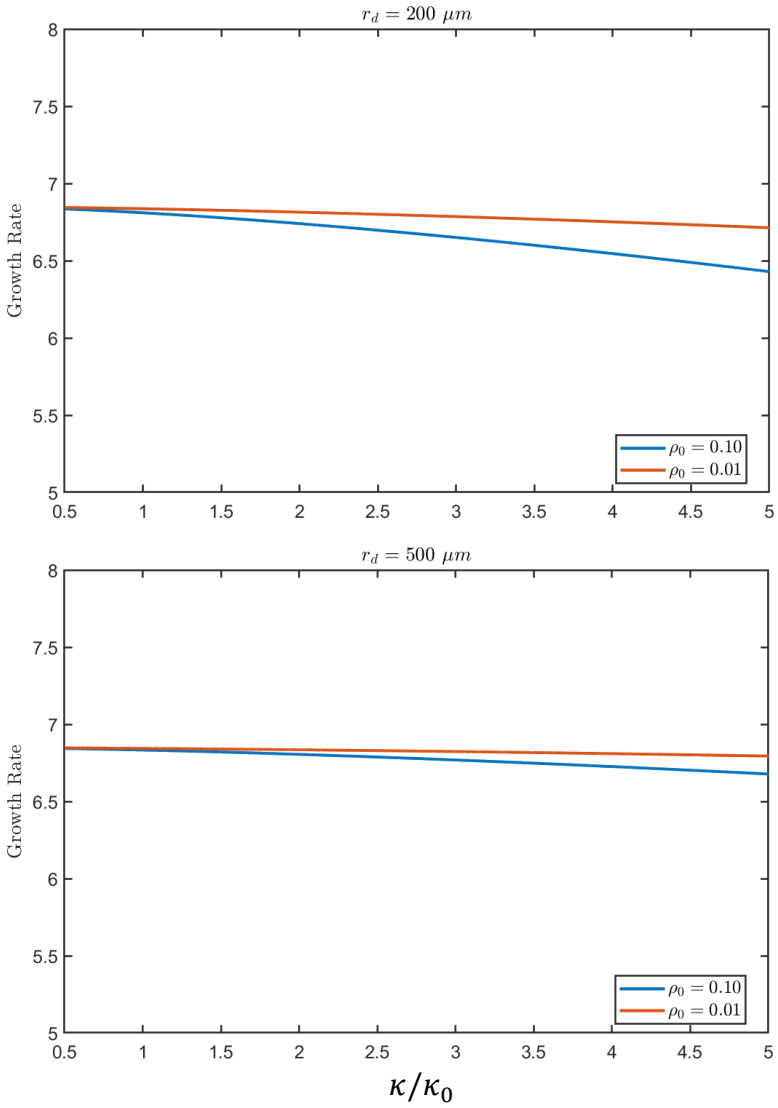

Fig. S8: Theoretical exponential growth rate of the ring pattern as a function of dipole strength at two inner radii r_d of the tube and under two bacterial densities (unit μm^{-3}).

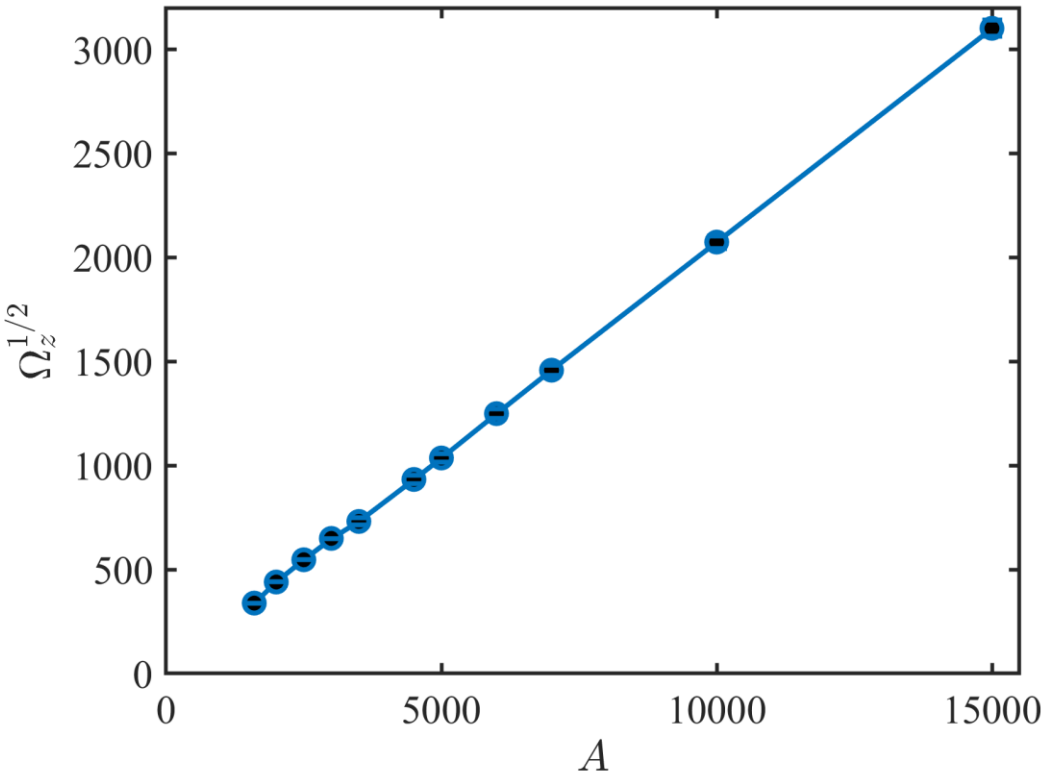

Fig.S9: Square-root of the enstrophy scales linearly with the activity parameter in simulations.